Results in Surfaces and Interfaces 25 (2026) 100986

Contents lists available at ScienceDirect

Results in Surfaces and Interfaces

journal homepage: www.elsevier.com/locate/rsurfi

Full length article

Differences in the reduction kinetics of thin RuO_2 layers in atomic and molecular hydrogen revealed by in situ photoemission

Ester Perez-Penco [a], Stefan van Vliet [a], Roland Bliem [a,b,*]

[a] Advanced Research Center for Nanolithography, Science Park 106, Amsterdam, 1098 XG, The Netherlands
[b] Van der Waals–Zeeman Institute, Institute of Physics, University of Amsterdam, Science Park 904, 1098 XH Amsterdam, The Netherlands

ARTICLE INFO

Keywords:
Reduction
Ruthenium oxide
Hydrogen
Radical chemistry
Nanolithography

ABSTRACT

The evolution of thin RuO_2 layers on Ru(0001) during exposure to atomic and molecular hydrogen was compared using *in situ* X-ray photoelectron spectroscopy (XPS) to improve the understanding of hydrogen uptake and the kinetics of oxide reduction. Time-resolved O 1s spectra separate a hydrogen-induced hydroxyl component from the intrinsic RuO_2 line shape obtained after anhydrous oxidation. The different peak position compared to bridging surface OH in literature, the large OH peak area, and its small probing depth dependence suggest the formation of subsurface OH species during H* exposure. During H_2 exposures at 2.5×10^{-5} mbar, mild hydroxylation is observed at room temperature and at 80 °C, but it proceeds slowly and saturates after <30 min. Exposure to atomic hydrogen cracked at the same H_2 background pressure yields significantly larger hydroxyl peaks, which continue to increase slowly even after more than three hours. At 105 °C, a 4.5 nm thick oxide layer is removed within 200 min by H_2, whereas the oxide is removed in approximately 20 min by atomic hydrogen. The different (sub)surface species and their time evolution support prior reports that assign hydrogen splitting as rate-limiting step for low-temperature reduction of RuO_2 by H_2, while highlighting that, for H*, oxygen mobility may already be relevant significantly below the reported peak temperature of water desorption.

1. Introduction

Ruthenium is a versatile material with applications ranging from catalysis [1–4] to nanolithography technology [5]. Its chemical stability in challenging environments and limited absorption of extreme ultraviolet (EUV) light make Ru a suitable choice for protective coatings in EUV lithography, for example for lithography masks [6–10]. Even small amounts of Ru surface oxidation by air, water, or oxygen exposure [11] are prevented in EUV lithography setups by operation in vacuum in a hydrogen background. The combination with EUV light generates hydrogen plasma [12], which helps maintain self-cleaning conditions inside the lithography tool [5,13,14]. The individual components of hydrogen plasma (hydrogen gas, radicals, and ions) are expected to contribute differently to the cleaning process and involve different rate-limiting steps in the reduction process that change with the surface temperature.

In the study of Ru surface redox chemistry, the oxidation of Ru metal has received considerable attention, motivated by the promising catalytic properties of Ru oxides, for example for oxygen evolution [15,16] and low-temperature dehydrogenation reactions [3]. At the Ru(0001) surface, the reaction with oxygen proceeds via the formation of various ordered adsorbate superstructures at (sub-)monolayer coverages [17,18], succeeded by an intermediate oxide layer that is electronically and structurally different from bulk rutile RuO_2 [19–23], which converts to a RuO_2(110) layer upon exceeding a critical thickness [21,24]. The reduction of the stable RuO_2 phase has also been studied using experimental techniques [25–30] such as X-ray photoelectron spectroscopy (XPS), scanning tunneling microscopy, temperature programmed reaction, surface X-ray diffraction, and low-energy electron diffraction, as well as computationally using density functional theory (DFT) calculations [26,27,31]. In molecular hydrogen, the reduction of RuO_2(110) is reported to be highly temperature-dependent at low pressures (1×10^{-5} mbar H_2), it is reported to have a threshold temperature of 127 °C [30]. Ugur et al. studied the reduction with molecular hydrogen in the range of 175–300 °C, reporting full oxide removal only above 200 °C [28,30,32]. With atomic hydrogen (H*), on the other hand, the efficiency of reducing the RuO_2(110) surface was found to be higher by one order of magnitude [29]. In the temperature range of 60–200 °C, the majority of thin oxide layers was reported to be removed within minutes of H* exposure, however, without reaching full reduction [13,29,33].

* Corresponding author.
E-mail address: r.bliem@arcnl.nl (R. Bliem).

https://doi.org/10.1016/j.rsurfi.2026.100986
Received 24 April 2026; Received in revised form 11 August 2026; Accepted 17 September 2026
Available online 22 September 2026
2666-8459/© 2026 The Authors. Published by Elsevier B.V. This is an open access article under the CC BY license (http://creativecommons.org/licenses/by/4.0/).

The mechanism of the reduction of RuO_2 by H_2 was proposed to proceed in 3 stages [28,29]. Initially, H_2 is dissociated at the surface, leading to the formation of surface hydroxyl groups (OH) passivating the uncoordinated O_{br} atoms. Attaching an additional hydrogen atom to a hydroxyl group yields a water molecule, which then re-accommodates to a coordinatively unsaturated Ru site (Ru_{cus}), from which it desorbs. Temperature-programmed desorption (TPD) [34] studies, combined with high-resolution electron energy loss spectroscopy (HREELS) [35], indicate a desorption temperature of around 127 °C for water on RuO_2(110). Knapp et al. find a similar value of 137 °C in TPD and temperature programmed reaction studies of heavy water over RuO_2(110) by different doses of D_2 [36] and of D_2 and O_2 [32]. The desorption of the water molecule creates an oxygen vacancy gradient perpendicular to the surface, triggering outward diffusion of oxygen from deeper layers. This oxygen vacancy exchange mechanism has been described as crucial in enabling the continuation of RuO_2 reduction in XPS studies based on three different oxygen species at the surface (oxidic, OH, and H_2O) [28,29]. However, despite convincing evidence for the peak position of bridging hydroxyls at the surface [32], the XPS peak shapes of anhydrous and hydroxylated Ru oxide layers remain ambiguous. This is potentially related to hydrogen uptake in the subsurface region, but real-time information on the extent of hydroxylation, its kinetics, and possible modifications of XPS peak positions is still lacking.

Here, we provide insight into the time-dependent effect of atomic and molecular hydrogen on Ru oxide layers. In situ monitoring of the ruthenium and oxygen core levels during oxidation and reduction allows assigning the peak position of the hydroxyl components and following the extent of hydroxylation with time. The evolution of the oxide and hydroxide components during hydrogen exposure is directly linked to the rate-limiting steps in the reduction of RuO_2 and sheds light on the nature of the residual oxygen after reduction.

2. Methods

A Ru(0001) single crystal was prepared in ultra-high vacuum (UHV, base pressure below 1.0×10^{-9} mbar) by annealing for 1 h at 600 °C, followed by oxidation of the Ru(0001) in 1.2×10^{-4} mbar of oxygen at 300 °C, and reduction again at 700 °C in UHV. The oxide layers for reduction were prepared at an oxygen pressure of 1.2×10^{-4} mbar for 105 min at 410 °C, as measured by a SensorTherm M322 two-color pyrometer. This yielded ruthenium oxide layers of 3.8 to 5.0 nm thickness, calculated from XPS peak intensities of the metallic and oxidized components of the Ru 3d level assuming a homogeneous flat oxide overlayer [37]. The same approximation was used to calculate the remaining oxide and oxygen coverages in monolayers. A detailed description of the thickness and monolayer calculation is provided in the Supporting Information. During the reduction experiments, the temperature was measured using an N-type thermocouple in contact with the manipulator, which was calibrated using an N-type thermocouple clamped directly onto a sample plate. The reduction of the RuO_2 layers was investigated using near-ambient pressure XPS with a Scienta Omicron HiPP-3 spectrometer with a 1.0 mm entrance slit and a monochromatic Al Kα X-ray source (1486.6 eV). XPS peak fitting was performed using KolXPD. Survey spectra were acquired at a pass energy of 500 eV; Ru 3d and O 1s spectra at 100 eV for high-resolution *in situ* spectra. The reduction experiments were performed in 2.5×10^{-5} mbar of hydrogen (Cangas, 99.999% purity). Atomic hydrogen was generated using an Oxford Applied Research TC-50 thermal gas cracker operated at 30 W. At this power, radiative heating from the cracker element increased the sample temperature to 40 °C as measured by the thermocouple. The dissociation fraction was not independently calibrated and is therefore not quantified. Throughout the manuscript, H* refers to hydrogen passed through the thermal cracker, i.e. a mixture enriched in atomic hydrogen. The reduction experiment at 105 °C was also reproduced under similar conditions using a SPECS PCS-ECR Plasma Source operated in hybrid mode without extraction voltage and with an ion trap. In the reference experiment on the effect of X-rays on reduction by H_2, the hydrogen supply was closed before starting the X-ray source for each data point and re-opened only after switching off the X-ray source. To quantitatively compare the reduction kinetics, the temporal evolution of the Ru^{4+}/Ru_{tot} ratio was fitted using the Johnson–Mehl–Avrami–Kolmogorov (JMAK) equation [38],

$$d(t) = d_\infty + \left(d_0 - d_\infty\right) \exp\left[-(kt)^n\right], \tag{1}$$

where $d(t)$ is the measured Ru^{4+}/Ru_{tot} ratio at time t, d_0 and d_∞ are the initial and final values of the ratio, respectively, k is an effective rate constant (min^{-1}), and n is the Avrami exponent. The fitting was performed by nonlinear least-squares regression using the `curve_fit` routine implemented in the SciPy Python library.

Although the JMAK equation was originally developed to describe nucleation and growth transformations, it is employed here as an empirical model for the progressive formation of metallic Ru during the reduction of RuO_2, in line with previous studies that successfully applied this approach to hydrogen-driven oxide reduction by describing the process as the nucleation and growth of the metallic phase [39,40]. As the reduction process involves several coupled steps, including hydrogen dissociation, oxygen removal, and water formation/desorption, the fitted Avrami exponent is not assigned a direct mechanistic interpretation. Instead, the extracted effective rate constant k is used as a quantitative parameter to compare the reduction kinetics under molecular (H_2) and atomic hydrogen (H*). Effective rate constants were extracted only for the reduction curves acquired at 105 °C, as these were the only datasets exhibiting continuous removal of the oxide. Consequently, an activation energy could not be determined from an Arrhenius analysis, which requires rate constants obtained over a range of temperatures.

3. Results

Before and during the reduction, the thin RuO_2 oxide layers grown on Ru(0001) were characterized using XPS of the Ru 3d and O 1s core levels. Fig. 1 shows the Ru 3d and O 1s spectra of the oxidized Ru surface before reduction (a, b) and during atomic hydrogen reduction at 80 °C (c, d).

In Fig. 1(a, c) the colored lines represent the individual fit components corresponding to metallic Ru (280.0 eV), oxidized Ru (Ru_{metal} + 0.65 eV), and the characteristic satellite peak for the rutile RuO_2 phase (Ru_{metal} + 2.7 eV), close to literature values [41,42]. The significant overshoot at high binding energies is an artifact of constraining the background while using an asymmetric peak shape for the Ru oxide component of the Ru 3d spectrum. Fig. 1(b, d) depicts the O 1s spectra, with the main peak corresponding to the Ru oxide at 529.4 eV. The satellite feature at O_{oxide} + 0.8 eV (fixed to 30% of the area of the main peak with a constant shape) was defined based on monitoring the oxide growth in situ during (anhydrous) oxidation. In situ reduction experiments during H* exposure at 40 °C and 80 °C show the gradual emergence of a distinct feature at approximately 531 eV with increasing hydrogen dose. Difference spectra of anhydrous and hydrogen-exposed oxide suggest an intensity maximum of the new feature at O_{oxide} + 1.6 eV. This binding energy is significantly higher than the established peak position for bridging surface OH at 1.1 eV [32], while remaining clearly below the literature value for molecular water at O_{oxide} + 2.8 eV, which we include as a separate species in the fit [32,36]. The contribution of this peak to the O 1s spectrum reaches more than 40% for the H*-exposed samples. Considering the mean free path of O 1s electrons excited by Al Kα radiation in RuO_2 of 1.99 nm, as calculated using the QUASES-IMFP software based on the Tanuma–Powell–Penn (TPP-2M) model [43], this high intensity clearly indicates that the signal originates from more than just the surface layer of the oxide. Angle-resolved XPS measurements up to 40° off-normal angle (see Supporting Information Figure S2) show little difference in the O 1s peak shape, providing further evidence that the hydrogen-induced

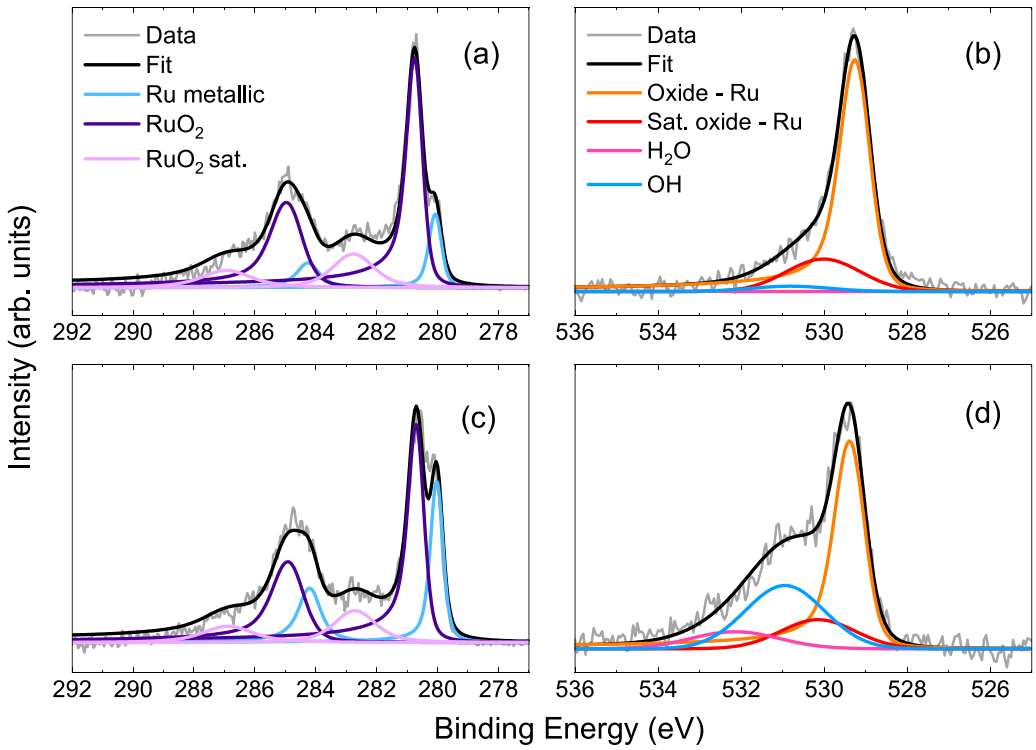

Fig. 1. High-resolution XPS spectra of the Ru 3d and O 1s regions of oxidized Ru(0001) before hydrogen exposure (a, b) and during exposure to H* at 80 °C (c, d).

feature at O_{oxide} + 1.6 eV is not localized to the surface. We thus assign this feature to subsurface hydroxyl groups that form upon sufficient hydrogen supply from the surface. The signal of the bridging surface hydroxyls is expected to contribute a maximum of 4.2% to the total O 1s signal at our experimental conditions and a layer thickness of 5 nm, assuming a density of bridging surface hydroxyls of 5 nm^{-2} and an O 1s mean free path in RuO_2 of 1.99 nm [30]. Given its proximity to the O 1s peak of Ru oxide and the subsurface hydroxyl peak, its low intensity, and the resolution of a lab-based spectrometer, we found it to be within the uncertainty of the fitting process, showing random variations from zero intensity to approximately 3.5% of the oxygen signal between data points in the time series. We did not include this species in the final fits, since it cannot be reliably assessed whether it is actually present during the reduction or removed during exposure.

3.1. *In situ reduction of RuO_2*

The ruthenium and oxygen spectra were followed as a function of time and sample temperature during the reduction of RuO_2 by 2.5 × 10^{-5} mbar hydrogen gas (H_2) and partially cracked hydrogen (H*). Fig. 2 shows the evolution of the Ru^{4+}/Ru_{tot} ratio, obtained from the metallic and oxidized components of Ru 3d during exposure to H_2 and H* without sample heating, and with the sample at 80 °C and 105 °C. The Ru^{4+}/Ru_{tot} ratio directly follows the reduction of RuO_2 by monitoring the fraction of Ru remaining in the Ru^{4+} oxidation state. While the oxide thickness obtained from the Ru 3d spectra provides a useful estimate of the oxide layer evolution, the Ru^{4+}/Ru_{tot} ratio offers a more direct measure of the Ru oxidation state and facilitates comparison with the O 1s analysis. It should be noted that changes in the Ru^{4+} fraction are not necessarily accompanied by an equivalent decrease in the total oxygen signal, as oxygen may remain in the system in hydroxylated species during the reduction. The time series of Ru 3d spectra for OH-rich layers shows a gradual decrease in fit quality with hydrogen uptake. Specifically, the fit remains lower than the data at approximately Ru_{metal} + 0.4 eV and the Ru_{metal} peak increases even though very little oxygen is removed. This indicates the emergence of a new, Ru–OH-related peak at an intermediate binding energy between the Ru_{metal} and RuO_2. To investigate this possibility, we introduced an additional Ru 3d spin–orbit doublet and systematically varied its position. The best agreement was obtained at Ru_{metal} + 0.25 eV. This peak indeed not only improves the fit and limits the variation in Ru_{metal} intensity but also follows a trend of increasing peak area with rising OH content in O 1s. The Ru^{4+}/Ru_{tot} ratio nevertheless remains unaffected to a good approximation, as it is referenced to the total peak area and is independent of the nature of the low-binding-energy species. However, the approach of a single symmetric Ru–OH species fails to provide a consistent quantitative description of the hydroxyl formation in the Ru 3d and O 1s regions, as discussed in detail in the Supporting Information (Figures S10–S12 and Table S1). This consistency could potentially be reached by defining more complex peak shapes, which is, however, not reliably achievable for the present data and would require a dedicated high-resolution study. Consequently, the following trends in reduction are discussed using a traditional model based only on the oxide and metal components.

The temperature difference without sample heating (20 °C for H_2 and 40 °C for H*) is due to the radiative heating of the surface by the hot cracker tube. It is not expected to affect the comparison of H_2 and H*, since even increasing the temperature up to 80 °C in H_2 does not induce any major change in the oxide layer. In this and all following figures, t = 0 represents the first spectrum acquired after starting the exposure to the reducing agent, while points at t < 0 show the initial state before reduction.

At 20 °C in H_2 (dark blue), no measurable change in the Ru^{4+}/Ru_{tot} ratio was observed, whereas in H* at 40 °C (light blue) it gradually decreased from 0.74 to 0.62 (a decrease of 0.12, corresponding to 17%) over 250 min. At an increased temperature of 80 °C, H_2 (dark green) and H* (light green) induced a gradual decrease in the Ru^{4+}/Ru_{tot} ratio by 7.4% and 16.2%, respectively. For these low temperatures, the reduction was slow and did not show any signs of saturation after 180 min. At 105 °C, however, a drastic change in the reduction

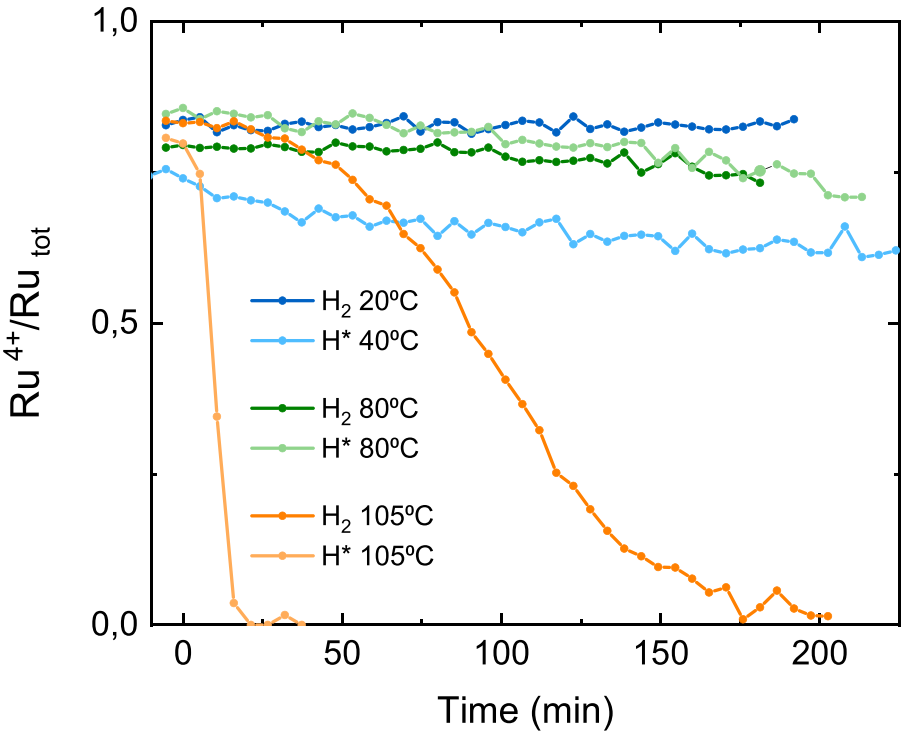

Fig. 2. Reduction curves showing the Ru^{4+}/Ru_{tot} ratio as a function of time (min). The reduction experiments were performed at different temperatures with 20 °C and 40 °C plotted in blue, 80 °C in green and 105 °C in orange, with dark and light colors representing H_2 and H*, respectively.

Table 1
Ru oxide layer thickness before and after reduction in H_2 and H* at different temperatures.

	Start oxide (nm)	Final oxide (nm)	Time (min)
H_2 20 °C	4.7	4.8	192
H_2 80 °C	4.3	3.7	181
H_2 105 °C	4.8	0.1	203
H* 40 °C	3.8	2.9	251
H* 80 °C	5.0	3.6	213
H* 105 °C	4.5	0	21

behavior was observed. H_2 exposure (dark orange) resulted in a slow initial decrease, followed by a faster reduction that led to an almost complete disappearance of the Ru^{4+} contribution after approximately 200 min, leaving behind approximately 45% of a monolayer of oxidized Ru. H* exposure at 105 °C (light orange) led to a rapid decrease in the Ru^{4+}/Ru_{tot} ratio in 21 min to a coverage below our detection limit of the oxide component. An overview of the initial oxide thicknesses, determined from the Ru 3d spectra, together with the corresponding reduction times is provided in Table 1. The variation in initial thickness is not expected to play a role in this reduction step, because the initial oxide is in the same phase, as evidenced by the comparable relative intensity of the Ru oxide peak and its satellite.

3.2. Oxygen species

To determine the effect of the different hydrogen species on the oxide surface chemistry in more detail, the time evolution of the three different oxygen species in the O 1s region was analyzed during exposure to H_2 and H*. Fig. 3 displays the time evolution of the total oxygen content (black dashed line) and the relative contents of the individual oxygen species during exposure to hydrogen gas (left) and radicals (right). The shaded regions represent the estimated fitting uncertainty of the O 1s components. These uncertainty bounds were obtained by systematically varying the OH component binding energy from pos(O–Ru)+1.5 eV to pos(O–Ru)+1.8 eV. At larger modifications, the data cannot be reproduced by the fits, as illustrated in the Supporting Information in Figure S1. The intensity of the Ru oxide peak and its satellite is shown in orange (O–Ru), the intensity attributed to hydroxyl groups (OH–Ru) in blue, and the water peak intensity (H_2O) in pink. All values are normalized to the respective total oxygen signal at $t < 0$, representing the initial surface state prior to the reducing agent. Immediately after oxidation the contributions from OH and H_2O species are minimal across datasets, represented in Fig. 3 by crosses at $t < 0$ (spectra provided in Figure S9). The crosses are omitted in panel (e) as the exposure to H_2 at 105 °C was performed on the surface previously exposed to H_2 at 20 °C, resulting in an initial OH contribution. The comparison of the crosses and the initial data points demonstrates that even short residence times in UHV at room temperature or during temperature stabilization lead to a slow but finite buildup of the OH signal in the O 1s region, while no change is discernible in Ru 3d. This change is likely due to the reported dissociation of hydrogen from the gas phase by bridging oxygen [44]. This behavior indicates a high reactivity of surface oxygen with low doses of hydrogen [32] from the residual gas but could also result from molecules activated by the voltage of the cold cathode pressure measurement cell. This observation highlights that even for oxides stored in ultra-high vacuum, the surface chemistry can vary significantly with storage time and residual gas species. This effect results in different offsets of the OH content before the hydrogen exposures, but does not affect the systematic trends reported for reduction and hydrogen uptake. For the H_2 exposure at 20 °C, an initial decrease in the O–Ru component is observed, whereas the Ru^{4+}/Ru_{tot} ratio remains essentially unchanged. The origin of this behavior cannot be conclusively determined from the present measurements. We speculate that the surface may be terminated by weakly bound oxygen-containing species after oxidation, which react with H_2 to form H_2O and desorb without affecting the Ru^{4+}/Ru_{tot} ratio. In the experiments at higher temperature, these species would already be removed by thermal desorption.

The time dependence of the oxygen components during H_2 exposure only shows a small increase in OH signal at 20 °C (a) and 80 °C

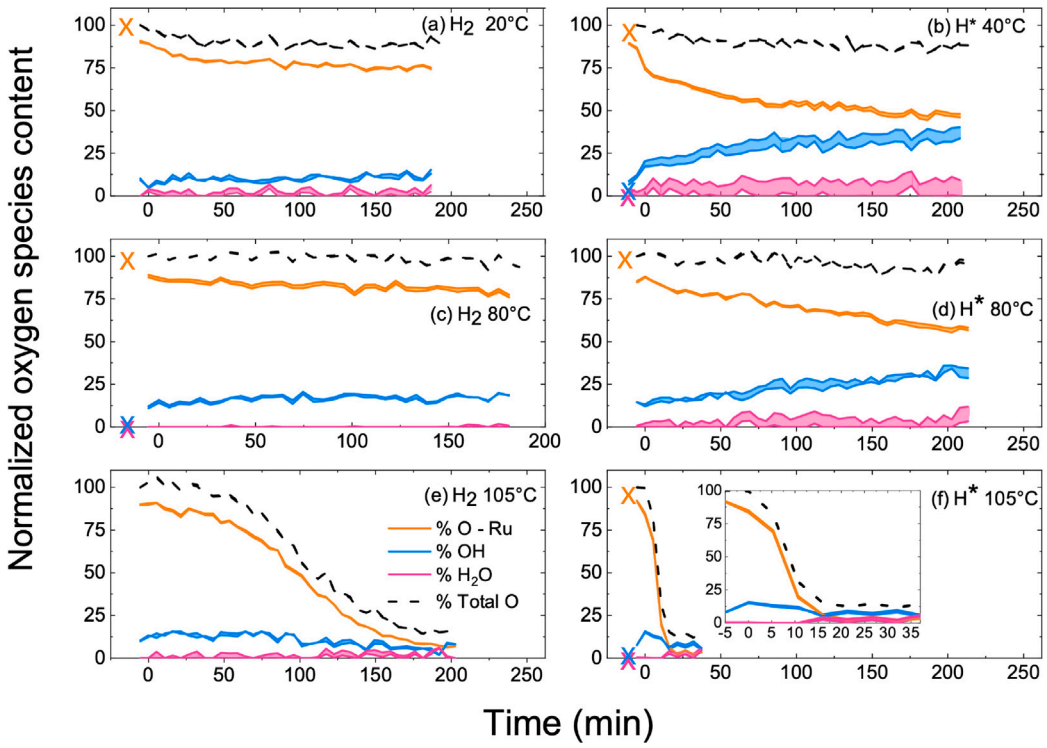

Fig. 3. Evolution of the three oxygen species (O–Ru, OH–Ru, H_2O adsorbate) during reduction of the RuO_2 layer. The *y*-axis denotes the relative content of each individual oxygen species. The shaded regions represent the estimated fitting uncertainty obtained from varying the position of the OH component from pos(O–Ru)+1.5 eV to pos(O–Ru)+1.8 eV.

(c), whereas at 105 °C (e) the intensity of the O 1s peak components from both oxide and hydroxide decrease and become comparable in intensity in the final stages of the reduction. No significant intensity in the H_2O region is discernible. To obtain a quantitative description of the reduction process, coverages and O:Ru ratios were determined from the fitted O 1s and Ru 3d peak intensities using the procedure described in the Methods section. After more than 200 min of reduction at 105 °C, a small amount of oxide signal (Ru^{4+}) remains in the Ru 3d region, estimated as approximately 45% of a monolayer of RuO_2 on Ru, while still 14.5% of the total initial oxygen signal is present. The ratio of O(O 1s): Ru^{4+}(Ru 3d) = 9.2 for the total O 1s content to the oxide component of the Ru 3d peak is clearly higher than the stoichiometry of any Ru oxide, indicating that a significant fraction of the oxygen is not part of the detected sub-monolayer oxide.

During H* exposure (Fig. 3(b, d, f)), the evolution of the oxygen species takes a different path. The initial decrease of oxide content is most pronounced at 40 °C, while the rate of conversion to OH becomes comparable for 40 °C and 80 °C at longer exposure times. We speculate that the H* recombination rate is increasing in contribution with increasing temperature, thus decreasing the uptake rate at higher temperature. When first layers are converted and diffusion to deeper layers is required, this process slows down the OH formation at 40 °C. The H_2O peak increases at the start of the reduction and quickly reaches a temperature-dependent average value of ≈8.1% for 40 °C and ≈2.7%, for 80 °C (average of the H_2O content of the last ten iterations), however, with the large uncertainty indicated by the width of the H_2O lines. Applying H* at 105 °C leads to a fast decrease of all species, while also following the trends observed at lower temperature. The oxide contribution decreases sharply and approaches that of the OH component at approximately 16 min. At the end of the reduction, no Ru^{4+} signal is present in the Ru 3d region. However, 14% of the total initial oxygen signal remains. The final peak area ratio of Ru 3d and O 1s is 1:8, corrected only for photoemission cross section. The hypothetical comparison of this ratio to an adsorbed overlayer of oxygen (see SI for details) yields an approximate coverage of 80% of a monolayer. Possible origins of this discrepancy are large uncertainties in determining small amounts of Ru oxide in a metal-dominated spectrum, possible changes in the oxidation state of Ru in a sub-stoichiometric oxide shifting the peak position, or high defect densities that provide strong adsorption sites for the remaining oxygen.

3.3. Quantitative analysis of the reduction kinetics

To perform a quantitative comparison of the reduction kinetics, the reduction curves obtained at 105 °C under atomic and molecular hydrogen were fitted using the Johnson–Mehl–Avrami–Kolmogorov (JMAK) equation, as described in the Methods section (Eq. (1)). The model accurately reproduces the experimental reduction profiles and yields effective rate constants of 0.089 min^{-1} and 0.009 min^{-1} for H* and H_2, respectively (Fig. 4). The effective rate constant obtained for atomic hydrogen is therefore approximately ten times larger than the one for molecular hydrogen, quantitatively confirming the substantially faster reduction observed experimentally. This pronounced difference supports the proposed mechanism in which hydrogen dissociation constitutes the dominant rate-limiting step during reduction by H_2, whereas this barrier is bypassed during reduction with atomic hydrogen.

3.4. Effects of X-ray irradiation on the reduction of RuO_2

The strong effect of activated species (H*) on the reduction of RuO_2 prompted an experimental test of the interference of the *in situ* measurement with its outcome. Fig. 5 shows a comparison of RuO_2 reduction in 2.5 × 10^{-5} mbar H_2 at 105 °C with (orange) and without (purple) simultaneous exposure to the Al Kα X-rays used by the spectroscopy tool. Keeping the X-ray source continuously on during hydrogen exposure results in the removal of the oxide layer in approximately 200 min. Even without continuous X-ray exposure, the

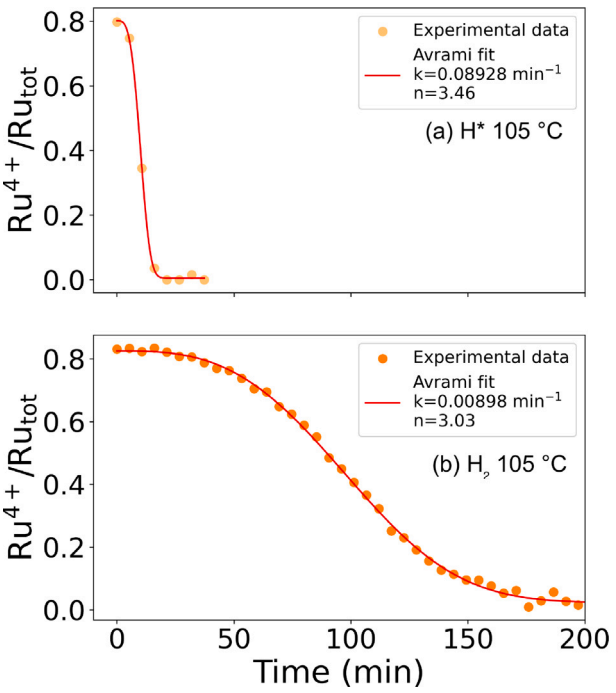

Fig. 4. Fits to the Ru^{4+}/Ru_{tot} reduction curves at 105 °C for (a) H* and (b) H_2.

RuO_2 layer is reduced, Ru^{4+}/Ru_{tot} = 0.03, corresponding to 0.13 nm of oxide and 16.2% of the original amount of oxygen remaining. However, irradiation with X-rays results in a substantial increase in the speed of reduction. We attribute the observed acceleration of the reduction to the activation of H_2 by secondary electrons [45,46], which aids the splitting of the hydrogen molecules (see Fig. 5).

4. Discussion

The *in situ* measurement of RuO_2 reduction provides new insights into the uptake of subsurface hydrogen, mechanistic differences between the reduction with atomic and molecular hydrogen, and the acceleration of the reduction process by ionizing radiation. Tracking the evolution of the core level spectra during hydrogen exposure allows us to assign an unambiguous peak position to the hydroxyl species within the layer, which shows only limited overlap with features of the anhydrous oxide. The curves presented in Fig. 3 illustrate a continuous increase in hydroxyl content in the presence of atomic hydrogen and confirm the expectation that the reduction of RuO_2 is progressively accelerated by increasing the temperature. At 105 °C, we observe oxide removal, with an oxide signal below one monolayer equivalent remaining for molecular hydrogen and below our detection limit for atomic hydrogen. For both reducing agents, the remaining oxygen content is smaller than the expected values from previously reported thicknesses after reduction at comparable conditions (0.25–0.6 nm [28,29]). However, even significantly longer exposures to hydrogen radicals did not further decrease the oxygen level. The continued presence of oxygen even after prolonged exposures could indicate the existence of highly stable oxygen adsorption sites, for example, on a rough, highly defective surface. Alternatively, the observation could be explained by the formation of a stable sub-oxide with a different Ru oxidation state and XPS peak position. The most likely explanation, however, is that small amounts of Ru-bound oxygen are partly reduced and become buried beneath metallic Ru, as suggested in prior studies on RuO_2 reduction [25,26], possibly comparable to subsurface oxygen formation in Ru oxidation [20].

The most striking differences between the reduction with H* and H_2 are revealed by the *in situ* analysis of the chemically different oxygen species (O–Ru, OH–Ru, H_2O). The relative contribution of the individual oxygen species remains similar throughout all exposures to H_2 at different temperatures, indicating that no excess hydrogen accumulates in the subsurface region and no additional OH groups or water are formed. Even at 105 °C, when reduction occurs, the ratios of the components show little change, indicating that the remaining oxide layer is unchanged and terminated with a thin hydroxylated layer. The formation of OH and H_2O is thus limited by the splitting of H_2, which no longer occurs in the absence of active surface oxygen species [44]. Exposure to H*, on the other hand, results in an increase of the peaks attributed to OH–Ru bonds and water at the expense of the O–Ru peak. The reactive H* species thus modify the oxide layer by generating hydroxyl groups, which continue to increase in density. Further addition of hydrogen to a hydroxyl group results in the formation of H_2O, which is present at H*-treated surfaces at 40 °C and 80 °C, exhibiting a negligible desorption rate close to room temperature. The initial decrease of the oxide and oxygen content at 40 °C, however, suggests that water desorption may occur on the timescale of the experiment at this temperature. However, the decrease saturates quickly and no more oxygen removal is observed, indicating that either the desorption of water or its re-accommodation in the preferred surface site for desorption is the rate-limiting step. At 80 °C the water content is lower than at room temperature. However, if this decreased water content were solely due to faster desorption, water would have to desorb at a rate comparable to its formation by reaction with H*, and reduction at 80 °C should proceed very fast. The evolution of the H_2O signal across the three temperatures provides further insight into the reduction mechanism. Faster water desorption becomes possible at 105 °C and the reduction rate increases substantially, while the water peak in XPS spectra drops below our detection threshold for both reducing agents. The comparison of the water signal across the three temperatures thus shows a gradual decrease rather than an abrupt change, indicating that already at 80 °C, water slowly leaves the surface, in agreement with the slow but continuous oxygen removal in Fig. 3d. To explain the lower water content during H* exposure at 80 °C, we exclude a limitation by hydrogen supply and discard water decomposition as unlikely. One possible alternative is that the replenishment of oxygen or OH groups to vacant surface sites [28,29] also plays a relevant role in limiting the oxygen loss well below the reported desorption temperature of water [34].

5. Conclusions

In summary, we compared the reduction of RuO_2 by H* and H_2 at temperatures ranging from 20 °C to 105 °C using *in situ* XPS to determine the uptake of hydrogen and study the reduction kinetics. The emergence of a clear additional feature in the O 1s region upon atomic hydrogen exposure after in situ oxidation allows us to assign a distinct peak to hydroxyl groups that only shows limited overlap with the peak shape of the oxide. Together with its large intensity and weak probing-depth dependence, the assignment of the additional O 1s feature suggests the formation of predominantly subsurface hydroxyl species, improving the ability to quantify hydroxyl formation during storage in vacuum and exposure to H* and H_2. While for both reductants, the oxide is mildly reduced at 80 °C and is removed at 105 °C, the hydroxyl content only becomes a major component of the oxygen signal during atomic hydrogen exposures. At high temperature, hydrogen cracking causes a dramatic acceleration of the reduction. Quantitative analysis of the reduction kinetics at 105 °C shows that the effective reduction rate under atomic hydrogen is approximately one order of magnitude higher than under molecular hydrogen, consistent with hydrogen dissociation being the rate-limiting step for H_2 reduction. The major differences in hydrogen uptake and reduction rate between atomic and molecular hydrogen indicate that hydrogen splitting is

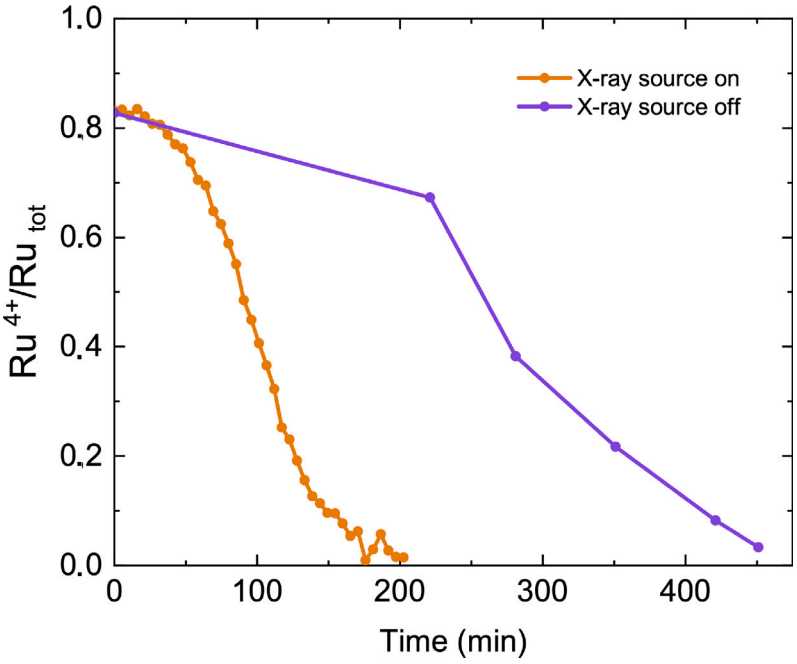

Fig. 5. Evolution of the Ru^{4+}/Ru_{tot} ratio during reduction in 2.5×10^{-5} mbar H_2 at 105 °C with (orange) and without (purple) simultaneous irradiation by X-rays.

the bottleneck for H_2 at all conditions. For reduction by H*, on the other hand, we propose, based on the relative intensities of hydroxide species and water, that the rate-limiting step transitions from water mobility and desorption at room temperature to the replenishment of surface oxygen by vacancy mediated diffusion at higher temperature. In the context of protective Ru coatings in plasma environment, our results highlight that RuO_2 layers are readily hydroxylated by hydrogen atoms at room temperature, but additional energy is needed to mobilize oxygen and maintain oxygen-free surfaces.

CRediT authorship contribution statement

Ester Perez-Penco: Writing – original draft, Investigation, Formal analysis, Data curation. **Stefan van Vliet:** Supervision, Methodology. **Roland Bliem:** Writing – review & editing, Supervision, Project administration, Funding acquisition, Conceptualization.

Declaration of competing interest

The authors declare that they have no known competing financial interests or personal relationships that could have appeared to influence the work reported in this paper.

Acknowledgments

This work has been carried out at the Advanced Research Center for Nanolithography, a public–private partnership of the University of Amsterdam, the Vrije Universiteit Amsterdam, the Dutch Research Council (NWO) and the semiconductor equipment manufacturer ASML.

Appendix A. Supplementary data

Supplementary material related to this article can be found online at https://doi.org/10.1016/j.rsurfi.2026.100986.

Data availability

Data will be made available on request.

References

[1] H. Over, Ruthenium dioxide, a fascinating material for atomic scale surface chemistry, Appl. Phys. A 75 (2002) 37–44.
[2] J. Aßmann, D. Crihan, M. Knapp, E. Lundgren, E. Löffler, M. Muhler, V. Narkhede, H. Over, M. Schmid, A.P. Seitsonen, et al., Understanding the structural deactivation of ruthenium catalysts on an atomic scale under both oxidizing and reducing conditions, Angew. Chem. 117 (6) (2005) 939–942.
[3] H. Over, Surface chemistry of ruthenium dioxide in heterogeneous catalysis and electrocatalysis: from fundamental to applied research, Chem. Rev. 112 (6) (2012) 3356–3426.
[4] J. Assmann, V. Narkhede, N. Breuer, M. Muhler, A. Seitsonen, M. Knapp, D. Crihan, A. Farkas, G. Mellau, H. Over, Heterogeneous oxidation catalysis on ruthenium: bridging the pressure and materials gaps and beyond, J. Phys.: Condens. Matter. 20 (18) (2008) 184017.
[5] H. Over, Y. He, A. Farkas, G. Mellau, C. Korte, M. Knapp, M. Chandhok, M. Fang, Long-term stability of Ru-based protection layers in extreme ultraviolet lithography: A surface science approach, J. Vac. Sci. Technol. B: Microelectron. Nanometer Struct. Process. Meas. Phenom. 25 (4) (2007) 1123–1138.
[6] P.-y. Yan, E. Spiller, P. Mirkarimi, Characterization of ruthenium thin films as capping layer for extreme ultraviolet lithography mask blanks, J. Vac. Sci. Technol. B: Microelectron. Nanometer Struct. Process. Meas. Phenom. 25 (6) (2007) 1859–1866.
[7] D. Thakare, J.-F. de Marneffe, A. Delabie, V. Philipsen, Ru/Ta bilayer approach to EUV mask absorbers: Experimental patterning and simulated imaging perspective, Micro Nano Eng. 20 (2023) 100223.
[8] D. Thakare, A. Delabie, V. Philipsen, Exploring the optimal combination of Ru/Ta bilayer mask stacks and illumination source shapes to mitigate mask 3D effects at high-NA extreme ultraviolet lithography, Opt. Express 32 (22) (2024) 38203–38223.
[9] B. Wu, A. Kumar, Extreme ultraviolet lithography: A review, J. Vac. Sci. Technol. B: Microelectron. Nanometer Struct. Process. Meas. Phenom. 25 (6) (2007) 1743–1761.
[10] N. Fu, Y. Liu, X. Ma, Z. Chen, EUV lithography: state-of-the-art review, J. Microelectron. Manuf 2 (2) (2019) 1–6.
[11] B. Herd, J.C. Goritzka, H. Over, Room temperature oxidation of ruthenium, J. Phys. Chem. C 117 (29) (2013) 15148–15154.
[12] M. van de Kerkhof, A.M. Yakunin, D. Astakhov, M. van Kampen, R. van der Horst, V. Banine, EUV-induced hydrogen plasma: pulsed mode operation and confinement in scanner, J. Micro/Nanopatterning, Mater. Metrol. 20 (3) (2021) 033801–033801.
[13] I. Nishiyama, H. Oizumi, K. Motai, A. Izumi, T. Ueno, H. Akiyama, A. Namiki, Reduction of oxide layer on Ru surface by atomic-hydrogen treatment, J. Vac. Sci. Technol. B: Microelectron. Nanometer Struct. Process. Meas. Phenom. 23 (6) (2005) 3129–3131.

[14] O. Braginsky, A. Kovalev, D. Lopaev, E. Malykhin, T. Rakhimova, A. Rakhimov, A. Vasilieva, S. Zyryanov, K. Koshelev, V. Krivtsun, et al., Removal of amorphous C and Sn on Mo: Si multilayer mirror surface in hydrogen plasma and afterglow, J. Appl. Phys. 111 (9) (2012).
[15] M.N. Iqbal, A.F. Abdel-Magied, H.N. Abdelhamid, P. Olsén, A. Shatskiy, X. Zou, B. Åkermark, M.D. Karkas, E.V. Johnston, Mesoporous ruthenium oxide: A heterogeneous catalyst for water oxidation, ACS Sustain. Chem. Eng. 5 (11) (2017) 9651–9656.
[16] H. Over, Y.D. Kim, A. Seitsonen, S. Wendt, E. Lundgren, M. Schmid, P. Varga, A. Morgante, G. Ertl, Atomic-scale structure and catalytic reactivity of the RuO_2 (110) surface, Science 287 (5457) (2000) 1474–1476.
[17] B. Herd, M. Knapp, H. Over, Atomic scale insights into the initial oxidation of Ru(0001) using molecular oxygen: a scanning tunneling microscopy study, J. Phys. Chem. C 116 (46) (2012) 24649–24660.
[18] J. Wintterlin, J. Trost, S. Renisch, R. Schuster, T. Zambelli, G. Ertl, Real-time STM observations of atomic equilibrium fluctuations in an adsorbate system: O/Ru(0001), Surf. Sci. 394 (1–3) (1997) 159–169.
[19] K. Reuter, M.V. Ganduglia-Pirovano, C. Stampfl, M. Scheffler, Metastable precursors during the oxidation of the Ru (0001) surface, Phys. Rev. B 65 (16) (2002) 165403.
[20] R. Blume, H. Niehus, H. Conrad, A. Böttcher, L. Aballe, L. Gregoratti, A. Barinov, M. Kiskinova, Identification of subsurface oxygen species created during oxidation of Ru(0001), J. Phys. Chem. B 109 (29) (2005) 14052–14058.
[21] J.T. Diulus, B. Tobler, J. Osterwalder, Z. Novotny, Thermal oxidation of Ru(0001) to RuO_2 (110) studied with ambient pressure x-ray photoelectron spectroscopy, J. Phys. D: Appl. Phys. 54 (24) (2021) 244001.
[22] A. Boettcher, U. Starke, H. Conrad, R. Blume, H. Niehus, L. Gregoratti, B. Kaulich, A. Barinov, M. Kiskinova, Spectral and spatial anisotropy of the oxide growth on Ru(0001), J. Chem. Phys. 117 (17) (2002) 8104–8109.
[23] A. Goriachko, H. Over, The nanostructuring of atomically flat Ru (0001) upon oxidation and reduction, Nanoscale Res. Lett. 11 (2016) 534.
[24] K. Reuter, C. Stampfl, M.V. Ganduglia-Pirovano, M. Scheffler, Atomistic description of oxide formation on metal surfaces: the example of ruthenium, Chem. Phys. Lett. 352 (5–6) (2002) 311–317.
[25] L. Atanasoska, W.E. O'grady, R.T. Atanasoski, F.H. Pollak, The surface structure of RuO_2: A LEED, auger and XPS study of the (110) and (100) faces, Surf. Sci. 202 (1–2) (1988) 142–166.
[26] H. Over, A.P. Seitsonen, E. Lundgren, M. Schmid, P. Varga, Experimental and simulated STM images of stoichiometric and partially reduced RuO_2 (110) surfaces including adsorbates, Surf. Sci. 515 (1) (2002) 143–156.
[27] H. Over, M. Knapp, E. Lundgren, A. Seitsonen, M. Schmid, P. Varga, Visualization of atomic processes on ruthenium dioxide using scanning tunneling microscopy, ChemPhysChem 5 (2) (2004) 167–174.
[28] D. Ugur, A. Storm, R. Verberk, J. Brouwer, W. Sloof, Kinetics of reduction of a RuO_2 (110) film on Ru(0001) by H_2, J. Phys. Chem. C 116 (51) (2012) 26822–26828.
[29] D. Ugur, A. Storm, R. Verberk, J. Brouwer, W. Sloof, Kinetics of reduction of a RuO_2(110) film on Ru(0001) by atomic hydrogen, Microelectron. Eng. 110 (2013) 60–65.
[30] Y. He, M. Knapp, E. Lundgren, H. Over, Ru (0001) model catalyst under oxidizing and reducing reaction conditions: in-situ high-pressure surface X-ray diffraction study, J. Phys. Chem. B 109 (46) (2005) 21825–21830.
[31] Q. Sun, K. Reuter, M. Scheffler, Hydrogen adsorption on RuO_2 (110): Density-functional calculations, Phys. Rev. B—Condensed Matter Mater. Phys. 70 (23) (2004) 235402.
[32] M. Knapp, D. Crihan, A. Seitsonen, E. Lundgren, A. Resta, J.N. Andersen, H. Over, Complex interaction of hydrogen with the RuO_2 (110) surface, J. Phys. Chem. C 111 (14) (2007) 5363–5373.
[33] R. Wasielewski, B. Yakshinskiy, M. Hedhili, A. Ciszewski, T. Madey, Surface chemistry of ru: relevance to optics lifetime in EUVL, in: 23rd European Mask and Lithography Conference, VDE, 2007, pp. 1–12.
[34] K.-T. Wang, S. Nachimuthu, J.-C. Jiang, Temperature-programmed desorption studies of NH_3 and H_2O on the RuO_2 (110) surface: effects of adsorbate diffusion, Phys. Chem. Chem. Phys. 20 (37) (2018) 24201–24209.
[35] A. Lobo, H. Conrad, Interaction of H_2O with the RuO_2(110) surface studied by HREELS and TDS, Surf. Sci. 523 (3) (2003) 279–286.
[36] M. Knapp, D. Crihan, A. Seitsonen, A. Resta, E. Lundgren, J.N. Andersen, M. Schmid, P. Varga, H. Over, Unusual process of water formation on RuO_2 (110) by hydrogen exposure at room temperature, J. Phys. Chem. B 110 (29) (2006) 14007–14010.
[37] A. Jablonski, J. Zemek, Overlayer thickness determination by XPS using the multiline approach, Surf. Interface Anal.: An Int. J. Devoted To Dev. Appl. Tech. Anal. Surfaces, Interfaces Thin Films 41 (3) (2009) 193–204.
[38] M. Avrami, Kinetics of phase change. I general theory, J. Chem. Phys. 7 (12) (1939) 1103–1112.
[39] Q. Jeangros, T.W. Hansen, J.B. Wagner, C.D. Damsgaard, R.E. Dunin-Borkowski, C. Hébert, J. Van Herle, A. Hessler-Wyser, Reduction of nickel oxide particles by hydrogen studied in an environmental TEM, J. Mater. Sci. 48 (7) (2013) 2893–2907.
[40] S. Pöyhtäri, J. Ruokoja, E.-P. Heikkinen, A. Heikkilä, T. Kokkonen, P. Tynjälä, Kinetic analysis of hydrogen reduction of nickel compounds, Met. Mater. Trans. B 55 (1) (2024) 251–265.
[41] D.J. Morgan, Resolving ruthenium: XPS studies of common ruthenium materials, Surf. Interface Anal. 47 (11) (2015) 1072–1079.
[42] C. Bianchi, V. Ragaini, M. Cattania, An XPS study on ruthenium compounds and catalysts, Mater. Chem. Phys. 29 (1–4) (1991) 297–306.
[43] S. Tanuma, C. Powell, D. Penn, Calculations of electron inelastic mean free paths. V. Data for 14 organic compounds over the 50–2000 eV range, Surf. Interface Anal. 21 (1994) 165–176, http://dx.doi.org/10.1002/sia.740210302,
[44] M. Knapp, D. Crihan, A.P. Seitsonen, H. Over, Hydrogen transfer reaction on the surface of an oxide catalyst, J. Am. Chem. Soc. 127 (10) (2005) 3236–3237.
[45] E. Böhler, J. Warneke, P. Swiderek, Control of chemical reactions and synthesis by low-energy electrons, Chem. Soc. Rev. 42 (24) (2013) 9219–9231.
[46] A. Houmam, Electron transfer initiated reactions: Bond formation and bond dissociation, Chem. Rev. 108 (7) (2008) 2180–2237.